Giant magnetoresistance due to orbital-symmetry mismatch in transition metal benzene sandwich molecules

Dongzhe Li[1,*] and Alexander Smogunov[2]

[1]*Institute for Advanced Study, Chengdu University, Chengdu 610100, People's Republic of China*

[2]*SPEC, CEA, CNRS, Université Paris-Saclay, CEA Saclay F-91191 Gif-sur-Yvette Cedex, France*

(Received 16 November 2020; revised 29 January 2021; accepted 8 February 2021; published 22 February 2021)

Achieving large magnetoresistance (MR) effects in atomic-scale junctions is of great importance in the field of molecular spintronics. In this work, using *ab initio* quantum transport calculations, we report on the spin transport properties of molecular junctions made of single transition metal benzene sandwich molecules ($TMBz_2$) bridged by ferromagnetic electrodes. We find that relative magnetic orientations of two electrodes and the molecule can dramatically affect low-bias transport properties of the junction. While the $TMBz_2$ are insulating in the gas phase, their corresponding molecular junctions bridged between the two electrodes are half-metallic minority-spin conductors (i.e., almost 100% spin polarization) and display very large MR. More interestingly, even larger molecular MR, corresponding to a reversal of molecular spin moment, are found due to the spin-valve behavior of the molecule controlled by the magnetic impurity. Such a particular performance is attributed to strong spin-selective hybridization of electronic states at the molecule/metal interface due to orbital-symmetry mismatch between the electrode's and molecular states. We also discuss the importance of the shape of electrodes on spin transport efficiency.

DOI: 10.1103/PhysRevB.103.085432

I. INTRODUCTION

The single-molecule junctions, where a single molecule is bridged between two metal electrodes, have become a versatile test bed for fundamental studies of electronic transport at the atomic scale [1]. Theoretical understanding and experimental realization of electron transport in single-molecule junctions, especially the control and manipulation of its degree of spin polarization, are currently of great importance in the field of molecular spintronics [2,3]. Magnetoresistance (MR) is a change in the resistance of a material system controlled by an applied magnetic field, which is recognized as the most important property that measures spin transport efficiency. In connection with molecular junctions, one can distinguish two types of MR. The first one is defined as the change in electrical conductance between parallel (P) and antiparallel (AP) magnetic orientations of two ferromagnetic electrodes, $\mathrm{MR} = (G_\mathrm{P} - G_\mathrm{AP})/G_\mathrm{AP}$. The second one, so-called molecular MR, is related to the change in relative spin orientation between electrodes and the molecule itself. Suggesting and designing possible molecular junctions producing as high as possible MR (ideally, infinite) is one of the most important goals in this field.

In pure ferromagnetic electrodes the current is largely dominated by *s* electrons in both spin channels (and generally a smaller contribution from spin-down *d* electrons) which makes it only partially spin-polarized, leading to limited spin-polarized current in the related nanodevices [4–6]. For instance, the spin polarization was found to be only about 33% in Ni atomic contacts [7], resulting in limited MR of about 40% [8]. In molecular junctions, unlike metallic contacts, the charge transport is mediated by localized molecular orbitals with different symmetries, possibly exhibiting unique transport behavior that cannot be observed in the pure atomic contacts or even the molecule itself. For example, M. Kiguchi *et al.* [9] have demonstrated that the electronic conductance of the Pt/benzene/Pt molecular junction is close to that of a metallic contact, although free benzene is a large-gap insulator. It has been also shown that spin filtering can be significantly enhanced by local incorporation of gas molecules during the formation of metallic contacts [10–12]. At the single-molecule scale, larger than 100% MR was predicted theoretically for $\mathrm{Fe}/\mathrm{C}_{60}/\mathrm{Fe}$ magnetic junctions [13]. Even larger MR of 200% was found in half-metal electrodes based molecular junctions [14]. An unexpected large MR up to 300% has been reported in spin valves based on Alq_3 [15]. A large and negative MR of about 50% is observed in combination with a high conductance in combined antiferromagnetic and ferromagnetic electrodes [16]. Moreover, it was demonstrated that the MR can be manipulated by a mechanical strain [12,17], anchoring groups [18,19], molecular geometrical torsion [20], and a protonation control [21]. For atomic nanocontacts, the values of giant MR of about 70% were reported recently for Co/Au/Co metallic junctions due to the strong perturbation of *s* states at Au contact atoms [22].

In the last two decades, two types of single-molecule junctions have been widely studied from both theory and experiment: i) ferromagnetic electrodes (such as Ni, Fe, and Co) bridged by a weakly coupled nonmagnetic molecule, in view of tunneling MR devices, making use of special orbital properties at the molecule/electrode interface for tuning their

*dongzhe.li1986@gmail.com

transport properties; ii) nonmagnetic electrodes joined by a small molecular magnet, where the spin transport is controlled by intrinsic magnetic properties of the molecule itself.

In the present work, we combine two approaches (both electrodes and a molecule are magnetic) by studying very simple magnetic molecules, formed by the Co transition metal ion between two benzene rings ($CoBz_2$ in the following), sandwiched between ferromagnetic Ni electrodes. Intense theoretical effort was invested in the understanding of the spin transport properties of transition-metal benzene ($TMBz_2$) molecules with nonmagnetic electrodes [23–27]. As one of $TMBz_2$ molecules, the $CoBz_2$ is readily synthesized by means of laser evaporation techniques. [28,29]. We calculate the electronic structure of molecular junctions as well as their transmission functions using the Landauer formula [30]. We find that, by changing relative spin configurations of electrodes and the molecule, low-bias transport properties can be significantly altered. Interestingly, while the $TMBz_2$ are insulating in the gas phase, their corresponding molecular junctions bridged between two electrodes are half-metallic conductors (i.e., almost 100% spin polarization) due to strongly spin-dependent electronic hybridization at the molecule-metal interface and, moreover, display very large MR effects. More interestingly, a spin-valve behavior provided by a single molecule is at the origin of even larger molecular MR–the change in conductance when the molecular spin moment is reversed. A detailed symmetry analysis shows that the hybridization between Ni-$d_{xz,yz}$ states, and the highest occupied molecular orbital (HOMO) of the $CoBz_2$ molecule (highly spin-selective due to orbital mismatch at the molecule/metal interface), is responsible for such huge MR effects. It turns out, moreover, that the "sharp" electrode terminations are important in order to obtain large MR due to tiny density of states (DOS) of spin-up d states at the Ni apex atoms around the Fermi energy.

II. THEORETICAL MODELS AND COMPUTATIONAL DETAILS

Spin-polarized electronic structure calculations have been performed using *ab initio* density functional theory (DFT) package SIESTA [31] within GGA approximation to exchange-correlation potentials (in PBE parametrization) [32]. We employed the DFT-D2 approach proposed by Grimme [33] to introduce long-range dispersion corrections. Molecular junctions were described in a supercell containing a single $CoBz_2$ molecule and two Ni(111) slabs with six atomic layers on both left and right sides. A 4×4 periodicity was used in the XY plane in order to avoid unphysical interactions between molecules due to periodic boundary conditions. The geometry relaxations were performed until the maximum residual force on each atom was less than 0.01 eV/Å. We used an energy cutoff for the real-space mesh of 300 Ry and a double ζ plus polarization (DZP) basis set with an energy shift of 50 meV, which resulted, as we have checked, in a good agreement with plane-wave code QUANTUM ESPRESSO [34] results (see Fig. 7 in Appendix A).

The coherent electron transport was studied by means of the quantum transport code TRANSIESTA [35], which employs a nonequilibrium Green's function (NEGF) formalism combined with DFT. The unit cell of the extended scattering region comprises $CoBz_2$ and three layers of electrodes on both sides. In the linear response regime, the ballistic conductance of each spin channel can be evaluated from the corresponding electron transmission function at the Fermi energy (E_F) using the Landauer-Büttiker formula formula:

$$G_\sigma = \frac{G_0}{2} T_\sigma(E_F), \tag{1}$$

where $G_0 = 2e^2/h$ is the conductance quantum (e being the electron charge and h Plank's constant) and $T_\sigma(E_F)$ is the transmission function for spin $\sigma = \uparrow, \downarrow$ at E_F. The total conductance is then defined as $G = G_\uparrow + G_\downarrow$.

The spin-resolved transmission function is evaluated using the NEGF formalism:

$$T_\sigma(E) = \mathrm{Tr}[\mathbf{\Gamma}_{L,\sigma} \mathbf{G}_{C,\sigma} \mathbf{\Gamma}_{R,\sigma} \mathbf{G}^\dagger_{C,\sigma}], \tag{2}$$

where $\mathbf{G}_C$ is the retarded Green's function of the central region (including the molecule and three layers of the left and right electrodes), while $\mathbf{\Gamma}_L$ and $\mathbf{\Gamma}_R$ are the coupling matrices of the central region to left and right leads, respectively. Here, the electronic structure calculations were carried out using a 6×6 $\mathbf{k}$-points mesh in the XY plane, while a denser 10×10 mesh was used for evaluation of the transmission functions.

III. RESULTS AND DISCUSSION

A. $CoBz_2$ in the gas phase

We start our discussion with the $CoBz_2$ molecule in the gas phase. We note that, when we relax the free molecule, the lowest energy configuration is the one with an asymmetric sandwich structure, in agreement with previous studies [26,36,37]. However, the molecule restores to its symmetric arrangement in the junction geometry, as will be discussed later. Therefore we show in Fig. 1 the calculated molecular level diagram in this symmetric geometry for both spin-up (black lines) and spin-down (red lines) channels. The HOMO-LUMO gaps are about 1.50 and 0.50 eV for spin-up and spin-down, respectively. The spin moment is found to be 1.0 μ_B, which is in good agreement with the previous theoretical study [25]. The distance of the Co atom to centers of benzene rings is about 1.76 Å.

For the spin-up, the HOMO is from $d^\uparrow_{z^2}$, while the LUMO is localized on two benzene rings (π-orbital) as is seen in Fig. 1. For the spin-down, the twofold degenerate HOMO is located at the central Co atom and originates from its $d^\downarrow_{xz,yz}$ orbitals, indicating a weak hybridization and strong atomic character. On the other hand, the LUMO, also twofold degenerate, is localized on benzene rings. Since only one electron should be accommodated on spin-down HOMO doublet, in gas phase the molecule gets deformed, as was mentioned above, a Jahn-Teller effect which leads to the HOMO splitting and lowers the total energy.

B. Ni chain/$CoBz_2$ junctions

When the molecule is contacted by metal electrodes, as in a mechanically controllable break-junction (MCBJ) or scanning tunneling microscope (STM) experiments, it interacts with the electrodes and their atomic structure will change. We find

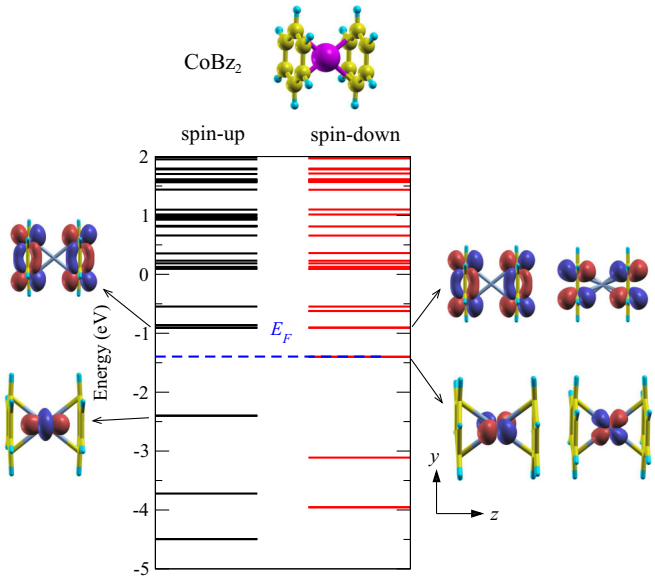

FIG. 1. DFT energy level diagram in the gas phase for a $CoBz_2$ molecule with a symmetric sandwich structure. Spin-up and spin-down components are plotted in black and red lines, respectively. The HOMO and LUMO for both spin channels are depicted together with their relative isosurfaces.

that the $CoBz_2$ restores to its symmetrical sandwich structure after atomic relaxations, no matter what is its initial configuration, which agrees with previous findings [26]. Therefore, the spin-down HOMO orbital remains almost degenerate and should be placed very closely to the Fermi energy (due to its one electron occupation). As a consequence, the electron transport will be presumably dominated by spin-down HOMO orbitals.

For the sake of simplicity, we first consider simple model-like systems in which one $CoBz_2$ molecule is sandwiched by two semi-infinite Ni monoatomic wires. In our transport modeling, the direction of the left electrode's magnetization is fixed, while the directions of the Co and right electrode are set to be ferromagnetic (FM)/antiferromagnetic (AFM) and parallel (P)/antiparallel (AP) with respect to the left electrode's magnetization, respectively, namely ↑↑↑, ↑↓↑, and ↑↑↓ spin configurations. We plot in Fig. 2 the spin-resolved energy-dependent transmission function, where the energy is measured with respect to the Fermi energy (E_F).

As described in Ref. [38], the ferromagnetic electrodes (i.e. Ni, Fe, or Co) possess at E_F very different spin populations: for spin-up, only states of orbital s symmetry are available (all the d states are fully occupied), while for spin-down, both s- and d-symmetry states are present. In the case of the ↑↑↑ configuration [see Fig. 2(a)] near E_F, the spin-up transmission is completely suppressed. In the spin-down channel (plotted in red), the transmission is dominated by two quasidegenerate HOMO orbitals originating from Co-$d_{xz,yz}$ states. Two available at the Fermi level spin-down Ni-$d_{xz,yz}$ channels have a perfect symmetry matching, with them resulting in the saturated transmission up to about 2. For the spin-up channel, the LUMO is strictly orthogonal to the only s-symmetry band of Ni nanowires, therefore the spin-up transmission (plotted in black) is completely blocked at the molecule-metal interface. As a result, a perfect spin filtering is observed, and the $CoBz_2$ plays therefore the role of half-metallic conductor.

Interestingly, in the ↑↓↑ configuration as shown in Fig. 2(b), the spin-down conductance is reduced considerably, by 90% compared to the case of the ↑↑↑. This can be understood by the fact that two dominating HOMO orbitals in the previous case, which are now of spin-up polarization, become completely decoupled from Ni nanowire states due to their orbital orthogonality to the Ni s-like channels only available at the Fermi energy. The residual spin-down conductance is due to the d_{z^2}-character molecular orbital at about -1.70 eV (corresponding to HOMO up in Fig. 1), which is rotationally symmetric and has thus a perfect overlap with Ni s states, providing a rather constant tunneling transmission of about 0.1 at the Fermi level. Therefore, when the local spin moment

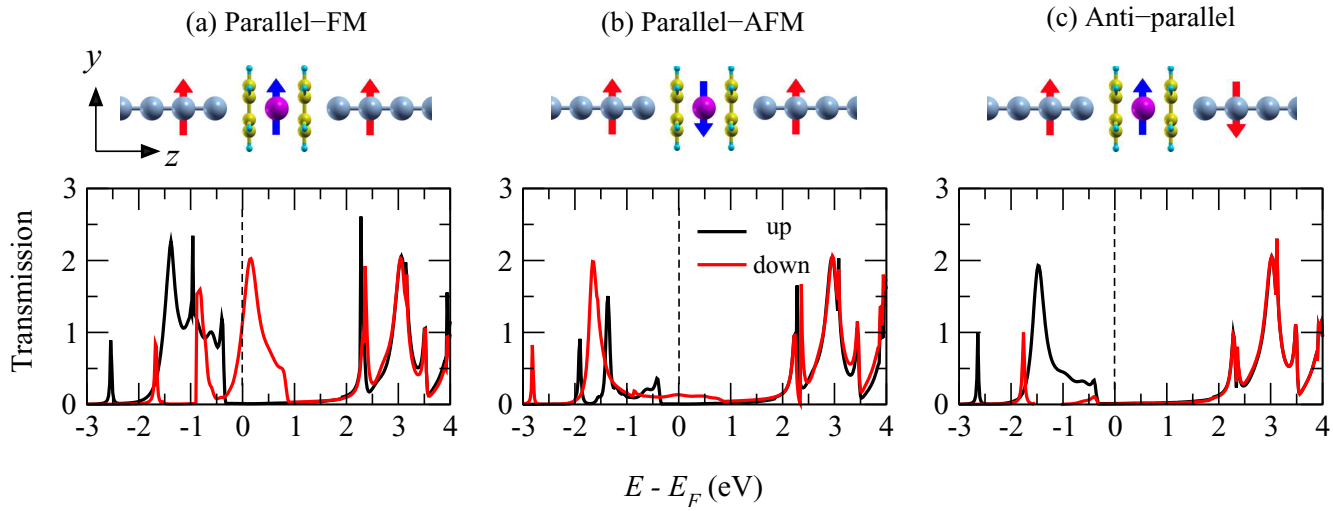

FIG. 2. Ni chain/$CoBz_2$ junctions: Spin-polarized transmission spectra for $CoBz_2$ single-molecule bridging the two semi-infinite 1D chains as shown on the inset in the top panels with three different spin configurations, namely ↑↑↑ (a), ↑↓↑ (b), and ↑↑↓ (c). Black and red lines denote spin-up and spin-down channels, respectively.

of Co is rotated, the $CoBz_2$ turns into almost an insulator, resulting in a large molecular MR of about 762%.

Furthermore, if two electrodes have AP magnetic alignment (↑↑↓, see Fig. 2(c)), the spin-down electrons passing through the left electrode/junction interface and propagating via the two HOMO orbitals will be reflected at the right molecule/electrode interface having antiparallel magnetic alignment. A very tiny spin-up transmission remains the same as for ↑↑↑ configuration so that the conductance is fully quenched for both spin channels, resulting in very high MR.

We find therefore that $CoBz_2$ suspended between Ni electrodes behaves as an excellent single-molecule spin valve that presents a perfect spin filtering and an infinite MR. Moreover, when two electrodes have P magnetic alignment, the current flow can be efficiently controlled by the magnetization of the molecule, resulting in a spin-valve behavior with extremely large MR.

We have also checked that the position of principal conducting orbitals, spin-down HOMO, does not change essentially upon inclusion of possible correlations on the Co d shell treated at the DFT + U level (see Appendix B), so that our main conclusions on MR properties of junctions should remain unchanged.

C. Ni(111)/$CoBz_2$ junctions

Encouraged by our results for model-like systems, we now study more realistic junctions with Ni nanowires replaced by fcc-Ni(111) electrodes. Here, a single $CoBz_2$ is bridged with four-atoms pyramid-like electrodes as shown in Fig. 3. For the ↑↑↑ configuration, as in the model case, a remarkable difference of transmission curves for the two spin channels is observed (see Fig. 3(a)). The transmission coefficient for the spin-up channel is almost quenched with a tiny conductance of $G_\uparrow = 0.03G_0$. In contrast, for spin-down electrons, we find a significant and broad transmission peak located between −0.3 eV and 0.8 eV showing its maximum at E_F, the corresponding conductance is about $G_\downarrow = 0.95G_0$, which is almost saturated. The large spin-down broadening indicates strong hybridization between HOMO orbitals and Ni-$d_{xz,yz}$ states due to perfect orbital matching. Overall, we also find a good spin-filtering (of about 94%) for this realistic junction, though it is not as perfect as for the model case with semi-infinite Ni nanowires. However, in both ↑↓↑ and ↑↑↓ configurations [Figs. 3(b) and 3(c)], the transmission functions near E_F differ significantly from the model case. In particular, rather sharp spin-up/spin-down resonance just above E_F is observed for ↑↓↑ / ↑↑↓ magnetic alignments. The calculated MRs are found to be about 153% and 150%, respectively. Therefore, the emergence of a half metallicity (a fully spin-polarized current) does not necessarily translate into very large MRs. All our results are summarized in Table. I.

In order to understand the origin of the sharp spin-up transmission peak in the ↑↓↑ configuration, we plot in Fig. 4(a) the spin-up projected density of states (PDOS) on Ni apex atom, since it provides the information on the nature of incoming conduction channels. Here, the dashed and solid lines represent the Ni s and $d_{xz,yz}$ orbitals, respectively. Clearly, the PDOS is dominated by the s orbital, but a very small amount of relevant $d_{xz,yz}$ states are also present around the

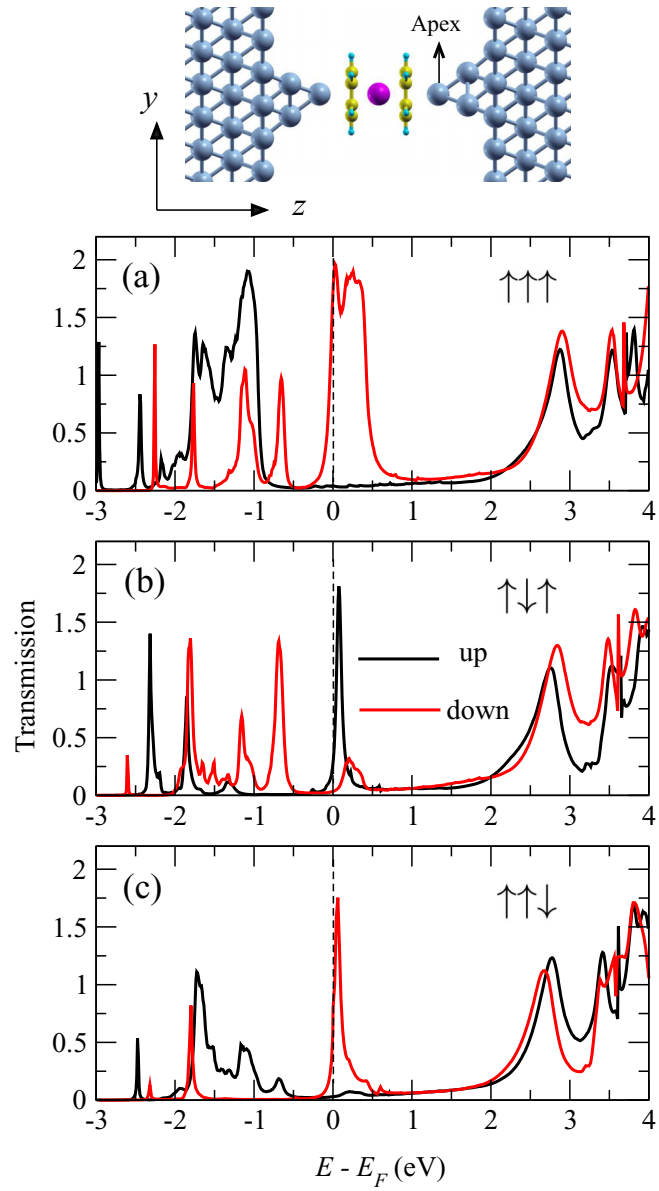

FIG. 3. Ni(111)/$CoBz_2$ junctions: Spin-polarized transmission spectra for $CoBz_2$ bridging two Ni(111) electrodes as shown on the top panel: (a) ↑↑↑, (b) ↑↓↑, and (c) ↑↑↓ spin configurations. The distance between a Ni apex atom and the Co atom is 4.0 Å. Black and red lines denote spin-up and spin-down channels, respectively.

Fermi energy, because of the breaking of axial symmetry. That results in the sharp transmission peak from spin-down HOMO (derived from Co-$d_{xz,yz}$ orbitals) observed in Fig. 3(b). In the model case of Ni semi-infinite chains, due to axial symmetry, the important $d_{xz,yz}$ PDOS was strictly zero around E_F, only an s Ni band (of wrong symmetry) was available so that the spin-up conductance was fully quenched. The same mechanism applies for the ↑↑↓ case too, where the similar sharp transmission peak is observed but now in the spin-down channel (since the molecule magnetization is reversed). We note, moreover, that two molecular states located at about 0.7 eV and 1.0 eV, shown as dashed lines in Fig. 4(b), do not participate to electron transport due to their orthogonality

TABLE I. Spin-ddependent conductances in units of $G_0 = 2e^2/h$, spin polarization (SP) and magnetoresistance (MR) for molecular junctions with Ni wire, Ni(111) and adatom+Ni(111) electrodes. Note that MR_1 and MR_2 are defined as $MR_1 = (G_{\uparrow\uparrow\uparrow} - G_{\uparrow\downarrow\uparrow})/G_{\uparrow\downarrow\uparrow}$ and $MR_2 = (G_{\uparrow\uparrow\uparrow} - G_{\uparrow\uparrow\downarrow})/G_{\uparrow\uparrow\downarrow}$, respectively.

	Ni chain	Ni(111)	Adatom+Ni(111)
$G_{\uparrow}^{\uparrow\uparrow\uparrow}$ (G_0)	0.000	0.031	0.015
$G_{\downarrow}^{\uparrow\uparrow\uparrow}$ (G_0)	0.578	0.950	0.490
$G_{\uparrow}^{\uparrow\downarrow\uparrow}$ (G_0)	0.000	0.181	0.031
$G^{\uparrow\downarrow\uparrow}$ (G_0)	0.067	0.018	0.021
$G_{\uparrow}^{\uparrow\uparrow\downarrow}$ (G_0)	0.000	0.014	0.018
$G_{\downarrow}^{\uparrow\uparrow\downarrow}$ (G_0)	0.000	0.285	0.041
SP (%)	100	94	94
MR_1 (%)	762	153	871
MR_2 (%)	∞	150	736

(by symmetry mismatch) to the conduction Ni *s* channel (see Appendix C).

D. Adatom+Ni(111)/$CoBz_2$ junctions

We consider finally the case of "sharp" electrodes by connecting the $CoBz_2$ to pyramid-like Ni(111) electrodes with one more atom on both sides as shown in Fig. 5, intending to approach a model situation with Ni nanowires. Such kinds of junctions have been reported in several experiments. For instance, Yelin and coworkers [39] have realized the formation of longer 1D Pt chains by incorporating a single benzene molecule in MCBJ while Li *et al* [40] showed that atomically wired molecular junctions can be achieved in STM experiments. However, the formation of long 1D chain-like molecular junctions with 3*d* transition metals (e.g., Ni, Fe, and Co) remains still very challenging task, but shorter – just few atoms long – chains as in our case, could be presumably accessed experimentally. Transmission functions for three magnetic configurations are presented in Fig. 5. As expected, the results become closer to the model simulations. In particular, the sharp transmission peak near E_F disappears in both ↑↓↑ and ↑↑↓ configurations, resulting in almost quenched conductance similar to the case of 1D electrodes. This is attributed to progressively lower spin-up DOS on important $d_{xz,yz}$ Ni apex orbitals near E_F when the tip becomes sharper (more chain-like). As a consequence, giant MRs of about 871% and 734% are found in this geometry for ↑↓↑ and ↑↑↓ configurations, respectively, (see Table I).

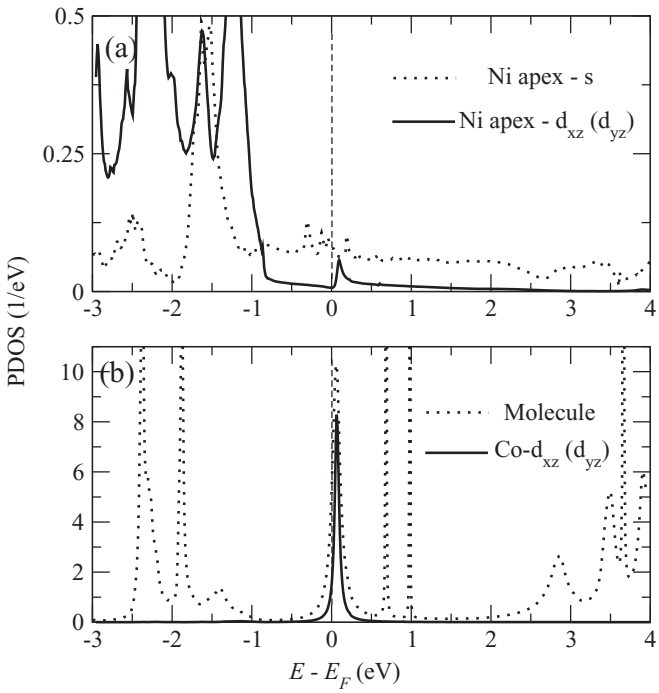

FIG. 4. Spin-up PDOS on Ni apex atoms (a) and molecule (b) for a Ni(111)/$CoBz_2$ junction in ↑↓↑ configuration as shown in Fig. 3(b). A sharp peak, originating from Co-$d_{xz,yz}$ and Ni-$d_{xz,yz}$, is found just above the Fermi energy.

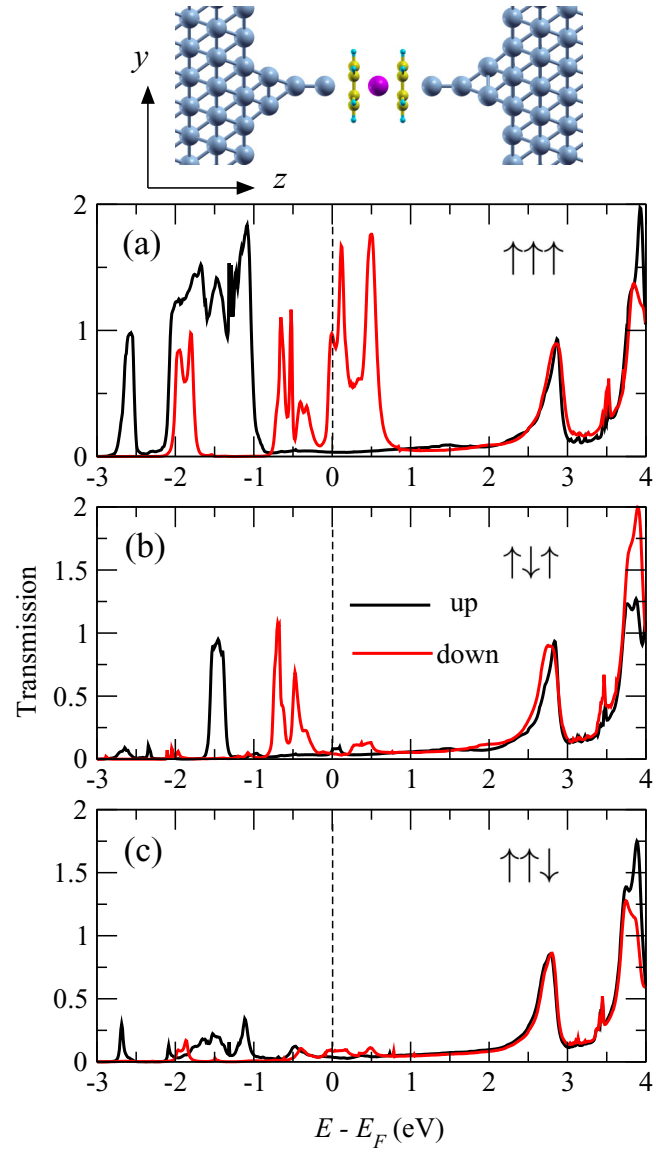

FIG. 5. Adatom+Ni(111)/$CoBz_2$ junctions: The same as Fig. 3, but with Ni(111) electrodes plus one outside atom connecting to the apex.

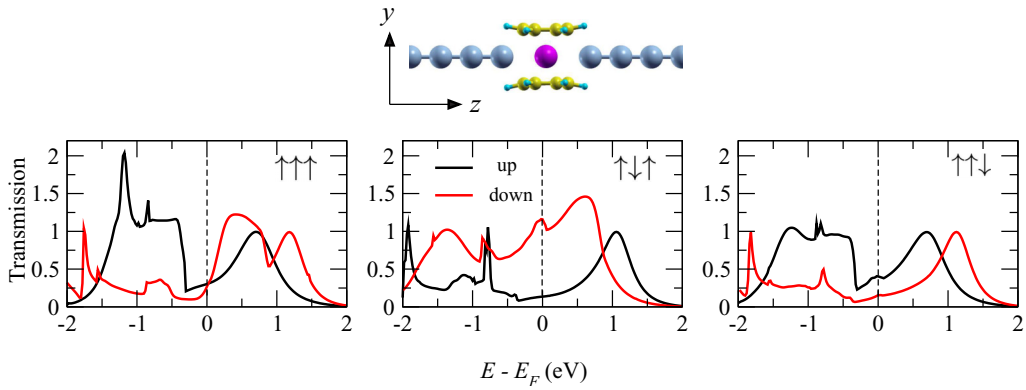

FIG. 6. The same as Fig. 2 but with perpendicular molecular connections.

Finally, to find out how the relative electrode-molecule orientation can change the overall spin transport, we investigate the case of perpendicular molecular orientation, as shown in Fig. 6. We find that the overall transport properties are very different from those in the parallel configuration studied before. The detailed electronic structure analysis shows that the conductance is now mediated not only by HOMO but has also significant contributions from d_{z^2}-character (the z refers always to the transport direction) molecular orbitals lying at higher energies. These orbitals, due to their symmetry and spatial orientation, couple very well to Ni-s states, while they were strongly decoupled in the parallel configuration. As a result, a moderate spin polarization of conductance in ↑↑↑ case is found and rather small MR values, $\mathrm{MR}_1 = -50\%$ and $\mathrm{MR}_2 = 5\%$, are predicted. Interestingly, MR_1 takes here the negative value, so that conductance measurements in two molecular configurations, if accessed experimentally, should reveal a pronounced difference. Note that similar sensitivity of spin filtering properties to the molecule orientation has been also reported recently for Ag/Vanadocene/Ag molecular junctions [41].

IV. CONCLUSIONS

To conclude, using a combination of density functional theory and nonequilibrium Green's function method, we have investigated the electronic structures and spin-dependent transport of a single $CoBz_2$ sandwiched between Ni(111) electrodes. We find that different magnetic configurations between electrodes and the molecule dramatically alter the low-bias transport properties of the junction. In the case of ↑↑↑, the junction yields 100% spin-polarized current, with a junction acting as a half-metallic conductor. The emergence of half-metallicity leads to a strong suppression of the current for AP alignment of the electrodes (↑↑↓), resulting in very large MR values more than 734%. Very interestingly, the current flow can also be efficiently controlled by the magnetization of the molecule (which can be rotated by a weak magnetic field, for example), being strongly suppressed in ↑↓↑ configuration, leading therefore to molecular MR as large as 871%. The physical mechanism behind these MR effects is the selective hybridization of electrode and HOMO orbitals at the molecule-metal interface, depending strongly on the electron spin polarization. Finally, it should be emphasized that the shape of the electrode can be important to optimize MR effects. We expect that the presented results can also apply for other benzene sandwich molecules and metallocene (two pentagon rings bound to a magnetic metal such as Co or Ni) molecule family possessing similar electronic structure and symmetries of frontier orbitals. We believe that our findings will provide practical guidelines for designing novel molecular nanodevices based on giant MR effects.

ACKNOWLEDGMENTS

D.L. acknowledges the financial support provided by the National Natural Science Foundation of China (Grant No. 12004054).

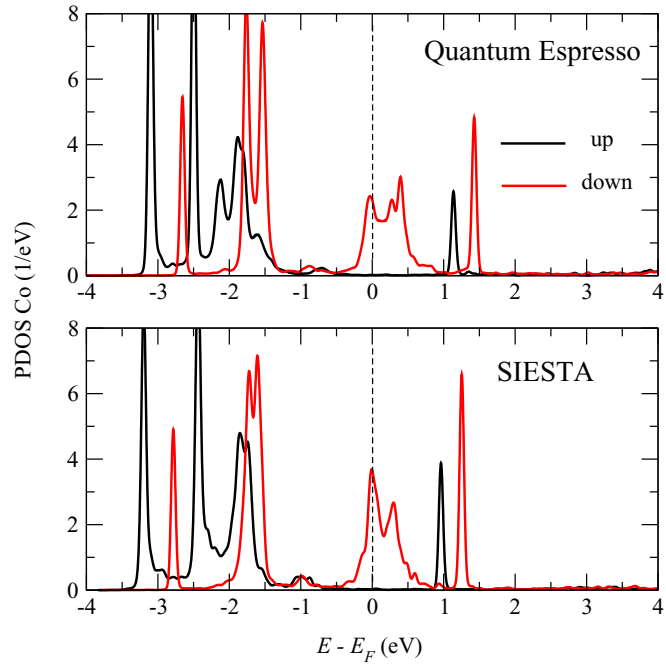

FIG. 7. Comparison between QUANTUM ESPRESSO (QE) and SIESTA results. Calculated spin-dependent PDOS on Co by QE (top) and SIESTA (bottom) for the Ni(111)/$CoBz_2$ junction with ↑↑↑ spin configuration. A good qualitative agreement is found between both sets of results, ensuring the accuracy of the basis sets parameters used in SIESTA.

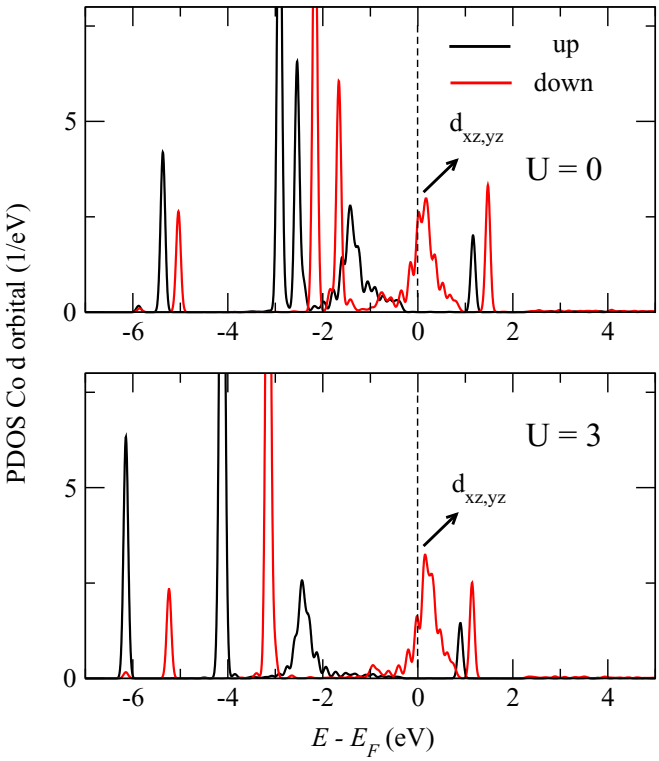

FIG. 8. Projected DOS of Co in Ni chain/$CoBz_2$ junction with ↑↑↑ calculated by DFT (top) and DFT + U (bottom).

APPENDIX A: COMPARISON BETWEEN QE AND SIESTA RESULTS

The reliability of the DZP basis sets parameters used in this work has been checked by comparing the electronic structure with plane-wave QUANTUM ESPRESSO (QE) [34] package. We plot in Fig. 7 the spin-resolved PDOS on Co using QE (top) and SISESTA (bottom). A good general agreement is found in terms of energy level alignment. The spin moment on Co is found to be about 1.30 μ_B and 1.26 μ_B for QE and SISESTA, respectively.

APPENDIX B: DFT+ U CALCULATIONS

The standard DFT is known to underestimate the HOMO-LUMO gap and overestimate the conductance. Therefore, we have checked the electronic structure calculated with DFT+ U approach, setting $U = 3$ eV on the Co d orbitals to correct for possible local correlations. Such a correction to DFT generally shifts occupied or unoccupied d-derived orbitals to lower or higher energies, respectively, therefore increasing the HOMO-LUMO gap. We find, however, that the spin-down HOMO (originated from Co $d_{xz,yz}$ states) remain essentially at the same energy, very close to the Fermi level, as shown in Fig. 8, presumably due to molecule neutrality charge condition (one electron should be placed on the twofold degenerate HOMO). On the other hand, the corresponding spin-up orbitals are shifted down in energy by about 1 eV. Since the transport in our junctions is dominated by spin-down HOMO, we believe that our simple DFT results are reliable in the present case. Finally, one can argue that other more accurate treatments of molecular orbitals using, for example, the GW approach may be needed. However, it has been shown that GW corrections affect rather unoccupied orbitals (poorly described within the ground state DFT), while occupied levels (in particular, the HOMO) are only slightly altered [42]. Therefore, once again this can validate our predictions on enhanced MR based on clear and robust symmetry arguments applied to HOMO orbitals.

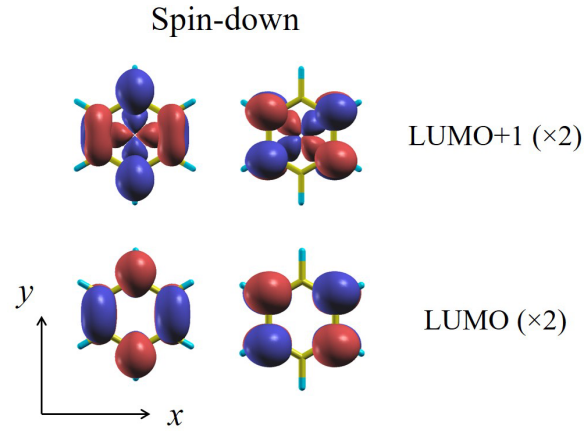

FIG. 9. Molecular orbital localization of spin-down LUMO and LUMO + 1 in the gas phase of $CoBz_2$ in the XY plane. These molecular orbitals will be orthogonal, by symmetry, to the s electrons of Ni electrodes.

APPENDIX C: MOLECULAR ORBITALS IN THE XY PLANE

We plot in Fig. 9 the wave functions for spin-down LUMO and LUMO + 1 in the XY plane. The plot allows us to rationalize that, due to orbital symmetry and shape, these molecular orbitals are strictly orthogonal to the s-symmetry states of contacting the molecule Ni electrodes.

[1] J. C. Cuevas and E. Scheer, *Molecular Electronics: An Introduction to Theory and Experiment*, Vol. 15 (World Scientific, Singapore, 2017).
[2] S. Sanvito, Chem. Soc. Rev. **40**, 3336 (2011).
[3] M. Sun and W. Mi, J. Mater. Chem. C **6**, 6619 (2018).
[4] D. Jacob, J. Fernández-Rossier, and J. J. Palacios, Phys. Rev. B **71**, 220403(R) (2005).
[5] M. Häfner, J. K. Viljas, D. Frustaglia, F. Pauly, M. Dreher, P. Nielaba, and J. C. Cuevas, Phys. Rev. B **77**, 104409 (2008).
[6] R. Vardimon, M. Matt, P. Nielaba, J. C. Cuevas, and O. Tal, Phys. Rev. B **93**, 085439 (2016).
[7] A. Smogunov, A. Dal Corso, and E. Tosatti, Phys. Rev. B **73**, 075418 (2006).

[8] Z. Razavifar, A. Saffarzadeh, and J. J. Palacios, Phys. Rev. B **101**, 235442 (2020).

[9] M. Kiguchi, O. Tal, S. Wohlthat, F. Pauly, M. Krieger, D. Djukic, J. C. Cuevas, and J. M. van Ruitenbeek, Phys. Rev. Lett. **101**, 046801 (2008).

[10] D. Jacob, J. Fernández-Rossier, and J. J. Palacios, Phys. Rev. B **74**, 081402(R) (2006).

[11] R. Vardimon, M. Klionsky, and O. Tal, Nano Lett. **15**, 3894 (2015).

[12] D. Li, Phys. Rev. B **99**, 174438 (2019).

[13] D. Cakir, D. M. Otálvaro, and G. Brocks, Phys. Rev. B **90**, 245404 (2014).

[14] X. Han, W. Mi, and X. Wang, J. Mater. Chem. C **7**, 4079 (2019).

[15] C. Barraud, P. Seneor, R. Mattana, S. Fusil, K. Bouzehouane, C. Deranlot, P. Graziosi, L. Hueso, I. Bergenti, V. Dediu *et al.*, Nat. Phys. **6**, 615 (2010).

[16] A. Bagrets, S. Schmaus, A. Jaafar, D. Kramczynski, T. K. Yamada, M. Alouani, W. Wulfhekel, and F. Evers, Nano Lett. **12**, 5131 (2012).

[17] Y.-H. Tang and C.-J. Lin, J. Phys. Chem. C **120**, 692 (2015).

[18] S. Qiu, Y.-Y. Miao, G.-P. Zhang, J.-F. Ren, C.-K. Wang, and G.-C. Hu, J. Magn. Magn. Mater. **479**, 247 (2019).

[19] D. Li, Y. J. Dappe, and A. Smogunov, J. Phys.: Condens. Matter **31**, 405301 (2019).

[20] S. Qiu, Y.-Y. Miao, G.-P. Zhang, J.-F. Ren, C.-K. Wang, and G.-C. Hu, J. Magn. Magn. Mater. **489**, 165465 (2019).

[21] S. Qiu, Y.-Y. Miao, G.-P. Zhang, J.-F. Ren, C.-K. Wang, and G.-C. Hu, J. Mater. Sci. **55**, 16311 (2020).

[22] I. N. Sivkov, O. O. Brovko, D. I. Bazhanov, and V. S. Stepanyuk, Phys. Rev. B **89**, 075436 (2014).

[23] H. Xiang, J. Yang, J. G. Hou, and Q. Zhu, J. Am. Chem. Soc **128**, 2310 (2006).

[24] J.-C. Wu, X.-F. Wang, L. Zhou, H.-X. Da, K. H. Lim, S.-W. Yang, and Z.-Y. Li, J. Phys. Chem. C **113**, 7913 (2009).

[25] M. Karolak, D. Jacob, and A. I. Lichtenstein, Phys. Rev. Lett. **107**, 146604 (2011).

[26] M. Karolak and D. Jacob, J. Phys.: Condens. Matter **28**, 445301 (2016).

[27] K. Lu, W. Gao, M. Xu, Y. Sun, J. Li, X. Yao, Y. Liu, and X. Zhang, ACS Omega **5**, 5534 (2020).

[28] M. Gerhards, O. Thomas, J. Nilles, W.-J. Zheng, and K. Bowen Jr, J. Chem. Phys. **116**, 10247 (2002).

[29] T. D. Jaeger, D. van Heijnsbergen, S. J. Klippenstein, G. von Helden, G. Meijer, and M. A. Duncan, J. Am. Chem. Soc **126**, 10981 (2004).

[30] Y. M. Blanter and M. Büttiker, Phys. Rep. **336**, 1 (2000).

[31] J. M. Soler, E. Artacho, J. D. Gale, A. García, J. Junquera, P. Ordejón, and D. Sánchez-Portal, J. Phys.: Condens. Matter **14**, 2745 (2002).

[32] J. P. Perdew, K. Burke, and M. Ernzerhof, Phys. Rev. Lett. **77**, 3865 (1996).

[33] S. Grimme, J. Comput. Chem **27**, 1787 (2006).

[34] P. Giannozzi, S. Baroni, N. Bonini, M. Calandra, R. Car, C. Cavazzoni, D. Ceresoli, G. L. Chiarotti, M. Cococcioni, I. Dabo *et al.*, J. Phys.: Condens. Matter **21**, 395502 (2009).

[35] M. Brandbyge, J.-L. Mozos, P. Ordejón, J. Taylor, and K. Stokbro, Phys. Rev. B **65**, 165401 (2002).

[36] J. W. Lauher, M. Elian, R. H. Summerville, and R. Hoffmann, J. Am. Chem. Soc. **98**, 3219 (1976).

[37] X. Zhang and J. Wang, J. Phys. Chem. A **112**, 296 (2008).

[38] A. Smogunov and Y. J. Dappe, Nano Lett. **15**, 3552 (2015).

[39] T. Yelin, R. Vardimon, N. Kuritz, R. Korytár, A. Bagrets, F. Evers, L. Kronik, and O. Tal, Nano Lett. **13**, 1956 (2013).

[40] J.-J. Li, M.-L. Bai, Z.-B. Chen, X.-S. Zhou, Z. Shi, M. Zhang, S.-Y. Ding, S.-M. Hou, W. Schwarzacher, R. J. Nichols *et al.*, J. Am. Chem. Soc. **137**, 5923 (2015).

[41] A. N. Pal, D. Li, S. Sarkar, S. Chakrabarti, A. Vilan, L. Kronik, A. Smogunov, and O. Tal, Nat. Commun. **10**, 5565 (2019).

[42] M. Strange, C. Rostgaard, H. Häkkinen, and K. S. Thygesen, Phys. Rev. B **83**, 115108 (2011).